Kinetics of viral load, immunological mediators and characterization of a SARS-CoV-2 isolate in mild COVID-19 patients during acute phase of infection

Running Title: Virus and inflammation in mild COVID-19 cases

Anbalagan Anantharaj[1*], Sunil Gujjar[1*], Saurabh Kumar[1*], Nikhil Jain[2], Jigme Wangchuk[1], Naseem Ahmed Khan[1], Aleksha Panwar[1], Akshay Kanakan[3], Vivekanand A[3,4], Janani Srinivasa Vasudevan[3], Asim Das[2], Anil Kumar Pandey[2], Rajesh Pandey[3] and Guruprasad R. Medigeshi[1]

1: Clinical and Cellular Virology lab and Bioassay Laboratory, Translational Health Science and Technology Institute, Faridabad, Haryana. INDIA.

2: Employees State Insurance Corporation Medical College and Hospital, Faridabad, Haryana, INDIA.

3: CSIR-Institute of Genomics and Integrative Biology, Delhi, INDIA.

4: Academy of Scientific and Innovative Research (AcSIR), Ghaziabad-201002, INDIA.

* These authors contributed equally

 # Corresponding author:

Guruprasad R. Medigeshi, PhD

Translational Health Science and Technology Institute,

NCR-Biotech Science Cluster,

P.O. Box # 4, Faridabad-Gurgaon Highway,

Faridabad 121001. INDIA.

Tel: +91-0129-2876311.

Email: gmedigeshi@thsti.res.in

ABSTRACT

Over 95% of the COVID-19 cases are mild-to-asymptomatic who contribute to disease transmission whereas most of the severe manifestations of the disease are observed in elderly and in patients with comorbidities and dysregulation of immune response has been implicated in severe clinical outcomes. However, it is unclear whether asymptomatic or mild infections are due to low viral load or lack of inflammation. We have measured the kinetics of SARS-CoV-2 viral load in the respiratory samples and serum markers of inflammation in hospitalized COVID-19 patients with mild symptoms. We observed a bi-phasic pattern of virus load which was eventually cleared in most patients at the time of discharge. Viral load in saliva samples from a subset of patients showed good correlation with nasopharyngeal samples. Serum interferon levels were downregulated during early stages of infection but peaked at later stages correlating with elevated levels of T-cell cytokines and other inflammatory mediators such as IL-6 and TNF- α which showed a bi-phasic pattern. The clinical recovery of patients correlated with decrease in viral load and increase in interferons and other cytokines which indicates an effective innate and adaptive immune function in mild infections. We further characterized one of the SARS-CoV-2 isolate by plaque purification and show that infection of lung epithelial cells (Calu-3) with this isolate led to cytopathic effect disrupting epithelial barrier function and tight junctions. Finally we showed that zinc was capable of inhibiting SARS-CoV-2 infection in this model suggesting a beneficial effect of zinc supplementation in COVID-19 infection.

IMPORTANCE

A majority of COVID-19 patients are asymptomatic or exhibit mild symptoms despite high viral loads suggesting a key role for the acute phase innate immune response in limiting the damage

and clearing the virus. Therefore, it is important to understand the early phase response to SARS-CoV-2 infection in such patients to devise strategies for clinical management of the disease. Our study shows the kinetics of immune mediators in the serum samples collected from hospitalized COVID-19 patients with mild symptoms. We further characterize a virus isolate from one of these patients and demonstrate its effect on epithelial barrier functions and show that zinc was capable of inhibiting SARS-CoV-2 infection under these conditions. Our results suggest a key role for the innate immune responses in the early phase of infection in mitigating clinical symptoms, clearing the virus and recovery from illness and suggest an antiviral role for zinc in COVID-19 infection.

Keywords: SARS-CoV-2; COVID-19; Cytokines; Chemokines; Inflammation; Zinc; epithelial cells.

INTRODUCTION

Coronavirus disease of 2019 (COVID-19) has infected over 35 million people worldwide leading to over a million deaths (as on 10th October 2020). Severe acute respiratory syndrome coronavirus-2 (SARS-CoV-2), a positive-sense RNA virus from the family *Coronaviridae* is the causative agent of COVID-19. The RNA genome of SARS-CoV-2 ranges from 26 to 32 kilobases in length and similar to other coronaviruses that have jumped species to infect humans, SARS-CoV-2 is believed to have been in circulation in animals such as bats for several decades before infecting humans (1). The genome of SARS-CoV-2 shares about 96% identity with that of bat coronavirus and is about 80% identical to the SARS-CoV-1 (2). Angiotensin converting enzyme-2 (ACE2) has been reported as a primary entry receptor for SARS-CoV-2 (3). ACE2, a type I membrane protein, is expressed in lungs, kidneys, intestine and heart. The spike glycoprotein (S-protein) on the SARS-CoV-2 virion surface mediates the receptor recognition and membrane fusion thus facilitating the entry of virus in the cell (4). There are close to 200 vaccines under development for COVID-19 and some of the vaccines have advanced to Phase III trials (5). Efforts to repurpose drugs and to manage the cytokine storm have identified a number of drugs that have been recommended for use in COVID-19 (6) but an effective antiviral specific to SARS-CoV-2 is yet to be licensed for human use.

Most of the patients with COVID-19 exhibit mild or no symptoms and severe clinical symptoms are observed in patients in the older age group (>65 years) or patients with underlying comorbidities such as hypertension and diabetes. Impaired immune response and cytokine storm has been implicated in clinical manifestations observed in severe disease (7-9). Increased viral load has been shown to correlate with disease severity (7, 10) and some of the antivirals such as

Remdesivir which inhibit the viral RNA-dependent-RNA-polymerase of SARS-CoV-1, Middle East Respiratory Syndrome Coronavirus (MERS-CoV) and SARS-CoV-2 has been shown to reduce time to recovery and mortality in COVID-19 patients (11). As is the case with RNA viruses, coronaviruses accumulate mutations and evolve at a rate similar to other RNA viruses (12, 13). Variations in the viral genome and emergence of novel clades has been implicated in increased fitness and transmission (14) however there is no evidence to suggest increased virulence of infecting virus as a cause of severe disease in COVID-19 patients suggesting that the host response and underlying comorbidities plays a key role in clinical outcomes (15). In this study, we monitored the kinetics of viral load in respiratory samples and saliva and cytokines and chemokines in the serum of hospitalized COVID-19 patients who displayed mild/moderate symptoms and recovered from illness. We isolated SARS-CoV-2 from one of the patients and further characterized the isolate by plaque-purification and sequencing and assessed the effect of virus infection on epithelial barrier functions. Our results suggest a clear inverse correlation between interferon response and viral load and identifies signatures in the inflammatory mediators in the serum of young patients who recover from COVID-19. We also show that the virus isolate from a patient with mild infection is capable of infecting lung epithelial cells and disrupting epithelial barrier functions leading to cell death further underscoring the importance of a robust host response in mitigating the clinical outcomes in COVID-19 infection. Finally, addition of zinc post-infection inhibited SARS-CoV-2 infection indicating the antiviral function of zinc in SARS-CoV-2 life-cycle.

MATERIALS AND METHODS

Human Ethics

The study was approved by the Institutional ethics committees for human research at both the institutions (No. 134/A/11/16/Academics/MC/2016/134 and THS 1.8.1/ (93)). Informed consent was obtained from all the participants.

Clinical samples

Patients with symptoms of COVID-19 infection were diagnosed using RealStar® SARS-CoV-2 RT-PCR kit (altona Diagnostics GmbH) at ESIC Medical College & Hospital. Clinical presentations were mild or asymptomatic (identified by contact tracing) and included mild to moderate fever, dry cough, and loss of sense of smell and taste. As per the regulations at the time of the study, all patients with a positive RT-PCR test were admitted to the hospital within 24-48 hours of testing positive and treated with azithromycin with hydroxychloroqine, Vitamin C and D. Samples were collected from patients who consented to participate in the study by signing the informed consent form. Nasopharyngeal/oropharyngeal (NP/OP) swab in virus transport medium (VTM), saliva and serum was collected from Day 1 of enrolment till discharge. Saliva was collected in specimen collection cups early in the morning immediately after the patient woke up from sleep. All the samples collected daily at same interval. All patients were isolated in the hospital for at least 14 days.

Virus culture and isolation

SARS-CoV-2 Isolate USA-WA1/2020 was obtained from BEI resources (deposited by the Centers for Disease Control and Prevention and obtained through BEI Resources, NIAID, NIH: SARS-Related Coronavirus 2, Isolate USA-WA1/2020, NR-52281). Indian isolates of SARS-

CoV-2 was isolated from COVID-19-positive VTM samples (VTM) using Vero E6 cells (Obtained from National Centre for Cell Science, Pune, INDIA). $2x10^6$ cells were grown in a T25 flask to about 80% confluency. Culture medium was removed and washed once with 5 ml of phosphate-buffered saline (PBS). 500 µl of VTM was added onto the cells and the flask was incubated for 1 h at 37ºC in a CO_2 incubator with intermittent mixing. After 1h of adsorption, monolayer was washed twice with 1X PBS and DMEM supplemented with 2% fetal bovine serum (FBS) and 2X antibiotics (200 units of penicillin, 200 µg of streptomycin) and 250 ng/ml amphotericin B and non-essential amino acids. Cell monolayer was observed under the microscope every day. Cytopathic effect was observed usually by day two of infection when the Ct value of the sample was less than 20 in RT-PCR. Culture supernatant was harvested and clarified at 1000 x *g* and multiple small aliquots were prepared and stored at -80ºC.Virus titer in the supernatants were estimated by plaque assays on Vero E6 cells as per the previous protocols (16) except that the cells were fixed at 60 h pi. Clinical specimens and virus cultures were handled in biosafety level 3 (BSL3) facility as per the standard operating procedure and guidelines for BSL3 level pathogen.

Quantitative RT PCR

RNA was extracted from 150 µl of VTM using Viral RNA Isolation Kit (MACHEREY-NAGEL), and eluted in 50 µl of nuclease-free water and used as a template for quantitation of SARS-CoV-2 viral RNA levels by reverse transcription polymerase chain reaction (RT-PCR). 2019-nCoV CDC Probe and Primer kit for SARS-CoV-2 manufactured (Biosearch Technologies) was used to detect N gene by real time RT PCR. RNAse P was detected as endogenous control for normalization. The region of N gene starting from 28287 – 29230 was

amplified using the forward primer 5'-GACCCCAAAATCAGCGAAAT-3' and the reverse primer 5'-GCGCGACATTCCGAAGAA-3' and cloned into pGEM®-T-Easy vector (Promega). This clone was linearized using Sac II enzyme and *in vitro* transcribed using the SP6 RNA polymerase (Promega). The transcript was purified and used as a template for generating standard curve to estimate the copy number.

For virus isolates, RNA was isolated from 4 different plaque-purified isolates using QIAamp Viral RNA mini kit (Qiagen) according to manufactures instruction. SARS-CoV-2 viral RNA was detected using RealStar® SARS-CoV-2 RT-PCR kit (altona Diagnostics GmbH). To check the presence of other respiratory virus in samples, FTlyo respiratory pathogen 21 plus kit was used (Fast Track Diagnostics). This detects presence of 21 respiratory viruses which includes influenza A virus; influenza A(H1N1) virus (swine-lineage); influenza B virus; human rhinovirus; human coronaviruses NL63, 229E, OC43 and HKU1; human parainfluenza viruses 1, 2, 3 and 4; human metapneumoviruses A/B; human bocavirus; human respiratory syncytial viruses A/B; human adenovirus; enterovirus; human parechovirus; *Mycoplasma pneumoniae* and 4 bacterial species *S. aureus*; *C. pneumoniae*; *H. influenzae* B; *S. pneumonia.*

Multiplex cytokine/chemokine assays

25 µl of serum was used for in magnetic bead-based multiplex chemokine and cytokine luminex assay as per the manufacturer's instructions (Merck-Millipore). Assays were performed in duplicates along with quality controls. The amount of each analyte was estimated by standard curve generated using known amount of analyte provided in the assay kit. Assay plates were read using MAGPIX system and data was analysed by xPONENT software using five parametric logistic fit model.

175

176 **Cell Viability assay**

177 Cell viability assay was performed using CellTiter-Glo® Assay kit (Promega) according to user
178 manual. Briefly, 20,000 Calu-3 cells were seeded in 96 well plate and grown for 48 h. Cells were
179 treated with zinc sulfate at indicated concentrations. After 24 h post treatment CellTiter-Glo
180 reagent was added to the well and luminescence was measured by microplate reader (Synergy
181 HT - BioTek).

182

183 **Labile zinc level measurement**

184 Labile Zn levels in the cells were estimated as described before (17). Briefly, after incubation
185 with zinc sulfate, cells were washed once with PBS, detached using trypsin and resuspended in
186 staining medium (DMEM without phenol red supplemented and with 2 mM L-glutamine; Gibco)
187 containing 2.5 μM ZinPyr-1 (ZP-1) (Santa Cruz) for 30 min at 37°C. Cells were washed using
188 fluorescence-activated cell sorter (FACS) buffer (PBS containing 0.25% FBS), and samples were
189 acquired in a FACS Canto II apparatus (Becton, Dickinson). The amounts of labile zinc present
190 in the cells are presented as the mean fluorescence intensities of ZP-1.

191

192 **Immunofluoresence**

193 VeroE6, Calu-3 (ATCC) and Caco-2 (ATCC) cells were seeded at 50,000 cells per well in 48-
194 well plate. Calu-3 and Caco-2 cells were seeded 2 days prior whereas VeroE6 were seeded a day
195 before infection. Cells were infected with SARS-CoV-2 THSTI-BL2010-D at 0.3, 1 and 3 MOI.
196 After 1 h of adsorption, viral inoculum was removed. Cells were washed twice with PBS. Cells
197 were kept in complete medium (10% FBS containing DMEM with penicillin, streptomycin and

glutamine mix and non-essential amino acids). At 24 h pi, cells were washed twice with PBS and once with cold PBS and fixed by using ice cold methanol and kept at -20ºC for 20 min. Methanol was removed, cells were washed once with cold PBS and then once with PBS at room temperature (RT), followed by blocking with 0.2% BSA-PBS for 10 min at RT. Cells were incubated with human chimeric SARS-CoV-2 S1 spike antibody (1: 100 dilution; Genescript – HC2001) in 0.2% BSA-PBS for 1h at RT. Cells were then washed three times with 0.2% BSA-PBS. This was followed by incubation with secondary antibody conjugated with anti-human Alexa flour 488 (1:500; Life Technologies–A11013) for 30 min at room temperature in dark. Cells were washed with PBS three times and stained with 4′,6-diamidino-2-phenylindole (DAPI) (Molecular probes) at 1:10,000 dilution for 10 min. Cells were washed with PBS and images were captured using Olympus DP80 microscope at 20X magnification. Images were processed by background subtraction using cellSens software. Bright field images were captured using Nikon Eclipse Ti-S at 10X magnification.

Zinc treatment

Calu-3 cells (40-50K) were seeded in a 24-well plate and two days post-infection, cells were infected with 0.3 MOI of SARS-CoV-2. Cells were cultured in serum-free MEM containing indicated concentrations of zinc sulfate for 24 hours. Viral titers in the supernatant was measured by plaque assays as described above.

Whole genome Sequencing and analysis

The protocol followed for the sample preparation, sequencing, and data analysis has been described earlier (18). In brief, double-stranded cDNA was synthesized from 50ng of total RNA

from virus stocks for all the four plaque-purified SARS-CoV-2 isolates. The first strand of cDNA was synthesized using Superscript IV followed by RNA digestion with RNase H for second-strand synthesis using DNA Polymerase I Large fragment (Klenow fragment). 100ng of purified double-stranded cDNA was taken for forward using ARTIC tiling PCRprotocol (V3 primer pools) (https://artic.network/ncov-2019) (19). 200ng of each purified sample of multiplexed PCR amplicons obtained was taken for library preparation using Oxford Nanopore Technology (ONT). This included End Repair/dA tailing, Native Barcode Ligation, and Adapter Ligation of the PCR amplicons. 100ng of the pooled and purified library was sequenced using ONT's MinION Mk1B platform (18).

Samples were base-called and demultiplexed using Guppy basecaller (version 3.5.2)(https://community.nanoporetech.com). Reads having phred quality score < 7 were discarded to filter the low-quality reads. The resulting fastq files were normalized by read length (300-500) and reads were aligned using Minimap2 (v2.17) (20) to the reference (GenBank: MN908947.3). Variants were called using Nanopolish(21)from the aligned reads and further creating consensus fasta using bcftools (v1.8). Finally, we used Nextclade (https://clades.nextstrain.org/) for the detection of clades from the consensus fastasequence.All the sequences are submitted to the GISAID database (https://www.gisaid.org/ ; GISAID EPI ISL - 454862).

Phylogenetic analysis

The consensus genomes obtained from the whole genome sequencing of 10 Indian isolates and four plaque-purified Indian isolates along with 86 other global SARS-CoV-2 sequences were used for constructing the phylogeny. The sequences were selected from a diverse geographical

location to represent the global distribution and spread of the virus. The sequences were obtained from the Global Initiative on Sharing All Influenza Data (GISAID) database. The fasta sequences were aligned using MUSCLE (22). A maximum-likehood Phylogeny was generated using FastTree 2.1.11 (23)with generalized time-reversible (GTR) substitution model and 1000 bootstrap replicates with default parameters. The tree was visualized and edited using ITOL (24).

Trans-epithelial electrical resistance and confocal microscopy

Calu-3 cells were grown in air-liquid interface as described elsewhere (25). Briefly, Calu-3 cells were seeded at 30,000 on 3 μm pore size transwell inserts (Corning - 3415). Cells were maintained at liquid-liquid interface for 7 days and cells were further grown with 600 μl of complete medium only in the basolateral compartment. Media was replaced every alternate day. TEER was monitored at indicated time points using a chop stick electrode (Millipore). On day 21 post-seeding, cells were infected with SARS-CoV-2-THSTI-BL2010D as described. At 24 h pi, culture inserts were washed with cold 1X PBS and incubated with cold methanol at −20°C for 20 minutes. Cells were further incubated with IMF buffer (20 mM HEPES, pH 7.5, 0.1% Triton-X-100, 150 mM sodium chloride, 5 mM EDTA and 0.02% sodium azide as a preservative) for 5 min at room temperature (RT) and all further washes were performed with IMF buffer. Non-specific antibody binding sites were blocked by incubating cells with IMF buffer containing 2% normal goat serum for 10 min at RT. Membranes were cut out using a scalpel blade and transferred to a 48-well plate. Cells were washed three times followed by incubation with antibodies against ZO-1 (Becton Dickinson), Claudin-3 (Invitrogen), SARS-CoV-2 spike antibody in IMF buffer (20 mM HEPES pH 7.5, 0.1% Triton X-100, 150 mM NaCl, 5 mM EDTA, 0.02 % sodium azide) for 1 h at RT. Cells were washed followed by incubation with

appropriate secondary antibodies tagged with Alexa fluor 488/568/633 (Molecular probes) for 30 min at RT by avoiding exposure to light. Cells were washed with IMF buffer three times and stained with DAPI at 1:10,000 dilution for 10 min. Cells were washed with PBS, mounted on glass slide using antifade solution (Molecular probes) and images were captured at 100X magnification using FV3000 confocal microscope (Olympus). Images were processed by background subtraction using cellSens software (Olympus).

Data analysis

Data was analysed and final graphs were prepared using GraphPad Prism (Version 7.0e) software. All experiments were performed with two or more replicates and graphs have been prepared representing data from at least two independent experiments with $n \geq 6$ unless otherwise indicated. Statistical significance was estimated by t-test (unpaired, non-parametric) using Mann-Whitney method.

RESULTS

Kinetics of viral load in COVID-19 patients with mild symptoms

11 patients who were positive for COVID-19 by RT-PCR were enrolled for the study after obtained informed consent. The median age of the patients was 32 (25% Percentile 24, 75% Percentile 45) and the mean duration of hospitalization was 14 days (Std. Dev. 4.034 days). Out of the 11 patients 6 were male and 5 were female. NP & OP swabs, saliva and serum samples collected for a maximum of 10 days. Most of the patients in this study manifested mild symptoms and were asymptomatic at the time of discharge. We measured daily viral load in the NP/OP samples by RT-PCR. For a subset of patients (n=5), we collected saliva samples early in

the morning for estimation of viral load in saliva and compare with the NP/OP sample. Viral load in NP/OP swab samples peaked between day 2 to 4 in most patients and we observed a biphasic increase in viral RNA levels in few patients with a second peak on day 5 (Figure 1A-1F). The peak viral RNA levels ranged from 10^6 to 10^{10} copies per ml of virus transport medium. Except for one patient, viral load in saliva correlated with viral load in VTM samples (Figure 1H-1K). In one patient, virus persisted in saliva till day 10 while the VTM sample was RT-PCR negative by day 6 of enrolment (Figure 1G). In most cases, the viral RNA was below the level of detection by RT-PCR by day 7-9 but two patients showed increasing trend in viral RNA levels although the last sample in these patients were on day 5 and day 7 (Figure 1D and 1H). These data suggest that the mild or asymptomatic patients harbour high viral load and salivary viral load can be a good alternate for the NP/OP swabs.

Kinetics of inflammatory mediators in mild/asymptomatic COVID-19 patients

As recent reports implicate both virus and host factors in severe COVID-19 disease, we were interested in estimating the levels of some of the inflammatory mediators along with interferons in the serum samples collected daily from mild COVID-19 patients to understand the correlates of recovery from disease. We measured 15 serum inflammatory mediators in each of the samples by multiplexing using luminex technology. The analytes detected are namely IFN-α2, IFN-γ, IL-1β, IL-4, IL6, IL-7, IL-8, IL10, IL12p40, IL12p70, IL17A, Monocyte Chemotactic Protein 1(MCP-1), MCP-3, TNF-α and gamma interferon inducible protein -10 (IP-10). We observed a consistent decrease in type I and type II during the acute phase of infection but both IFN-α2 and IFN-γ increased at later stages of infection coinciding with recovery and clearance of virus by day 8 of enrolment (Figure 2A). We next looked at the cytokines that influence T-cell functions

namely the pro-inflammatory IL-12p40 homodimer or IL-12p70, the active IL-12 heterodimer secreted by dendritic cells and macrophages that promotes Th1 response and leads to IFN-γ and TNF-α production. We observed a clear increase in IL-12p70 levels from day 5 onwards suggesting priming of T cells by the innate immune system through IL-12p70 secretion (Figure 2B). This increase coincided with increased IFN-γ levels observed in the same samples (Figure 1A). IL-7, a cytokine produced by epithelial cells and DCs and promotes biogenesis and proliferation of lymphocytes also showed an increasing trend coinciding with IL-12p70. However IL-17A levels did not show a significant change suggesting a more prominent role for Th1 responses in recovery in mild COVID-19 cases. Contrasting with the IFN responses, the levels of IL-8 was elevated at early stages of infection suggesting a key role for innate immune cells such as macrophages which produce IL-8 thus promoting neutrophil recruitment to the site of infection leading to resolution of infection. Interestingly, the levels of other two pro-inflammatory chemokines IP-10 and MCP-1 did not show any variation and MCP-3 levels were very heterogenous during the course of infection in any of the patients suggesting lack of severe inflammatory response in these patients (Figure 2C). IL-6, an acute phase reactant which is implicated in the severe manifestations of severe COVID-19 symptoms showed a moderate increase in multiple phases but TNF-α levels were unchanged in majority of the patients. The levels of IL-10, IL-4 and IL-1β showed an increasing trend in samples from day 5 - day 8 of infection suggesting the activation of T cells (Figure 2D). Overall our data suggests a prominent role for the innate immune response in clearance of virus infection/infected cells at early states of infection and priming of adaptive immune responses which probably lead to long-term protection from re-infection.

Isolation and characterization of SARS-CoV-2

Increased viral loads have been associated with severe disease by previous reports (7, 15). We were interested in understanding whether the virus isolates from mild or asymptomatic infection have altered ability to evade immune response and cause cellular damage. In order to isolate and characterize an Indian isolate of SARS-CoV-2, we used NP/OP swab samples from six COVID-19 patients whose samples had a Ct value of 20 or less by the diagnostic RT-PCR. Vero E6 cells were inoculated with NP/OP swab samples and culture supernatant was harvested on day 2 post-infection when cytopathic effect was evident to generate passage 1 virus. The process was repeated two more times to generate passage 2 and passage 3 viruses (Supplementary Figure S1). One of the passage 3 isolate, THSTI-BL2010-D, was further plaque-purified by isolating four individual plaques (THSTI-BL2010-A through D) and propagating further one more time in Vero E6 cells to generate a large stock of passage 5 virus for all experiments (Figure 3A). All the plaque-purified virus showed CPE at 72 h pi. All the plaque-purified viruses were negative for 21 respiratory viruses and 4 bacterial species including Mycoplasma as assessed by RT-PCR indicating lack of any secondary pathogens. Next, we performed plaque assays to compare the plaque morphology of plaque-purified virus on VeroE6 cell-monolayer with SARS-CoV-2 USA-WA1/2020 isolate.Both the isolates developed plaques at 60 h pi, however, the plaque-purified isolate produced a more homogenous plaque size and distribution as compared to the USA-WA1/2020 isolate (Figure 3B).

SARS-CoV-2 infection in human epithelial cell lines

Infection of SARS-CoV-2 in human cell lines depends on the expression of its receptor angiotensin-converting enzyme 2 (ACE2) and the host protease TMPRSS2 (26). To confirm the

infectivity of THSTI-BL2010-D in human cell lines, we infected Vero E6, Calu-3 and Caco-2 cells with increasing MOIs of the virus and stained for the presence of spike protein by immunofluorescence assay at 24 h pi. As expected, Vero E6 cells showed the maximum infection followed by Calu-3 cells and Caco-2 cells (Figure 4A). We next compared growth curve of SARS-CoV-2 Wuhan strain and THSTI-BL2010D in Vero E6 cells. Cells were infected with 0.1 MOI of both strains and supernatants were collected at 24, 48 and 72 h pi. Plaque assay results showed titres of Wuhan strain was a log higher than THSTI-BL2010D at 24 h pi whereas at 48 h pi virus titres with both strains were similar (Figure 4B). Virus titers showed a declining trend at 72 h pi most probably due to cytopathic effect.

Whole genome sequencing

To further characterize the plaque-purified isolates at molecular level, we isolated RNA from the plaque-purified virus stocks and subjected to whole genome sequencing. All the four plaque-purified virus RNA samples showed similar changes in the nucleotide positions with most changes in the ORF1a region leading to five non-synonymous and one synonymous change in the protein sequence (Table 1). THSTI-BL-2010-C sample had one additional mutation G27806T resulting in a synonymous change in ORF7b. Two non-synonymous changes were also observed in ORF1b and N regions (Table 1). Interestingly, none of the Indian isolates in our study showed D614G mutations observed elsewhere which is associated with increased infectivity (27).The slippery heptanucleotide sequence and the pseudoknot structure were not disrupted in any of the samples as per the sequence alignment compared to the reference genome (Accession ID: MN908947.3). The phylogenetic analysis of the 100 representative SARS-CoV-2 sequences from around the world (Supplementary Table S1) revealed clustering of sequences

382 into five major clades according to the GISAID nomenclature system (https://www.gisaid.org).
383 Sequences from all the 14 genomes from our study were subjected to phylogenetic analysis and
384 were assigned to clade 19A which along with the 19B clade forms the earliest clade which
385 originated from Wuhan and was prevalent in Asia during the initial months of the outbreak
386 (Figure 5). This suggests that the SARS-CoV-2 isolates reported in our study are genetically
387 more similar to the reference Wuhan sequence (GenBank: MN908947.3).
388
389 **SARS-CoV-2 infection disrupts epithelial barrier**
390 We were further interested to investigate the effect of THSTI-BL-2010D isolate infection on
391 epithelial barrier functions. Polarized Calu-3 cells grown on transwells were infected with
392 SARS-CoV-2 at 0.3 MOI. TEER was measured at 24 h pi and virus titers in the apical and
393 basolateral supernatants were estimated by plaque assays. We observed a 60% reduction in
394 TEER values as compared to mock at 24 h pi indicating disruption of epithelial barriers as a
395 result of cytopathic effect (Figure 6A). As expected, virus was present both in the apical and
396 basolateral samples due to disruption of cellular junctions and polarity (Figure 6B). Cells were
397 stained for virus spike protein, ZO-1 and claudin-3 antibodies to visualize infected cells and
398 staining pattern of these representative junctional proteins. We observed disruption of both ZO-1
399 and claudin-3 staining in virus-infected cells but not in mock-infected cells (Figure 6C)
400 suggesting that SARS-CoV-2 isolated from an mild/asymptomatic patient infects polarized lung
401 epithelial cells and causes damage to epithelial barriers due to cytopathic effect.
402
403 **Zinc supplementation affects SARS-CoV-2 infection *in vitro***

Addition of zinc along with the zinc ionophore pyrithione, which stimulates zinc uptake, was shown to inhibit SARS-CoV infection in Vero E6 cells (28). We were interested to use our cell culture system to assess whether zinc has an inhibitory effect on SARS-CoV-2 infection. We first determined cytotoxicity and uptake of zinc in Calu-3 cells by treating cells with different concentration of $ZnSO_4$ at 25, 50 and 100 μM for 24 h. We observed cytotoxicity beyond 50 μM $ZnSO_4$ in Calu-3 cells (Figure 6D). Zinc uptake was determined by staining cells with zinc fluorophore, ZP-1, at 4 h post-treatment. Cells treated with 25 μM of $ZnSO_4$ showed 25% increase in labile zinc levels whereas cells treated with 50 μM of $ZnSO_4$ shows 50% increase in labile zinc levels as compared to mock-treated control suggesting that these cells are capable of zinc uptake (Supplementary Figure S2). Cells were infected with SARS-CoV-2 at 0.3 MOI and cultured in the presence of 25 and 50 μM of $ZnSO_4$ for 24 h. At 24 h pi viral titres in the supernatant was determined by plaque assay. Zinc treatment showed over three-fold reduction in viral titers at 24 h pi as compared to untreated cells (Figure 6E) indicating the antiviral effect of zinc salts on SARS-CoV-2 infection in these cells.

Discussion

Of all the coronavirus epidemic/pandemic of recent past, COVID-19 has had the maximum impact on global health and economy. Although most of the individuals are asymptomatic or with mild symptoms, the disease affects the elderly and people with co-morbidities the most indicating a critical role for innate immune response in limiting the viral load and spread. Most asymptomatic or individuals with mild symptoms harbour high viral loads in their respiratory tract and contribute to disease transmission. Previous report suggested reduced interferon response in severe patients as compared to mild/moderate cases 8-12 days after the onset of

symptoms (7) and viral genetics was not found to correlate with severe disease (15). We focussed our efforts to monitor the kinetics of viral load and inflammatory mediators in the serum samples of hospitalized COVID-19 patients who displayed mild to no symptoms but were RT-PCR positive for SARS-CoV-2 during screening at the hospital or contact tracing. Most of our patients were enrolled within 48 hours of testing positive and are likely to be within the first week of exposure to the virus. In patients where we could detect viral RNA in saliva samples, the viral load in saliva correlated well with the same in VTM samples suggesting that saliva sample could replace NP/OP swabs which cause discomfort to patients during sample collection. Collection of saliva would also reduce the cost and time involved in sample collection for COVID-19 diagnosis and self-sampling by patients would reduce the risk of exposure for health care workers. The copy numbers of viral RNA, as estimated by quantifying the nucleocapsid gene region, varied by four orders magnitude suggesting multiple factors including the initial inoculum as a major determinants of viral load in the respiratory tract. Despite this huge variation in viral load, the clinical features and disease outcome did not vary as all patients were able to clear the virus and recover from the disease. This clearly suggests that a robust immune response in younger adults is capable to clearing the infection and age and imbalance in immune response could contribute to severe disease in older individuals and patients with co-morbidities. We observed that decrease in viral loads coincided with increase in IFN responses which is in agreement with observations made by other groups in *ex vivo*, cell culture and animal models where SARS-CoV-2 was shown to be a more potent inhibitor of IFN responses than SARS-CoV-1 (29, 30). Although our study does not have relative comparison between samples from different severities, we observed a consistent decrease in type I and type II during the acute phase of infection. Low serum interferons preceded respiratory failure in critical COVID-19

cases (7) whereas we observed an increase in both IFN-α and IFN-γ in all the patients who recovered and were discharged in our study clearly indicating a critical role for interferon responses in recovery from COVID-19. Increase in type I and II interferons indicate activation of T cells and NK cells in addition to the monocytes and macrophages which may contribute to the interferon levels. We have not assessed the levels of IFN-λ in these samples which is known to play a major role in antiviral response from epithelial cells (31). Our results show that there was moderate to no induction of pro-inflammatory cytokines or chemokines such as IL-6, TNF-α, IP-10 in any of these patients. We also observed, at later stages of infection, a trend showing increase in IL-10, IL-4 and IL-1β and IL-12p70 suggesting activation of T cells. Interestingly, IL-8, the primary chemoattractant for neutrophil recruitment has been shown to play an important role in acute respiratory distress syndrome (ARDS) and in recruitment of neutrophils to the site of injury in lungs in sepsis (32). We speculate that generation of high levels of IL-8 by the cells of innate immune system such as macrophages leading to activation of neutrophils which engage in viral clearance from the respiratory tract. Interestingly, neutrophils have been shown to play a crucial antiviral role in influenza A virus infection and in neurotropic coronavirus models such as mouse hepatitis virus (33). However, sustained levels of IL-8 may lead to ARDS observed in severe COVID-19 patients. Therefore, we hypothesize that regulation of IL-8 signalling and neutrophil activity could be an important determinant of clinical outcomes in COVID-19 patients.

An earlier study from India reported the isolation of SARS-CoV-2 from an Indian patient and its characterization (34). We got one step further and generate the first plaque-purified SARS-CoV-2 isolate from India. Plaque-purified SARS-CoV-2 revealed clear and homogeneous plaques on

Vero E6 monolayers compared to the Wuhan strain where the plaques were very heterogeneous in size. As robust and consistent plaque reduction neutralization titers (PRNT) depend on high quality plaque assays, we believe our virus strain will help in establishing PRNT assays that could work reliably and consistently and help vaccine studies. Although SARS-CoV-2 primarily targets the respiratory system, *in vitro* and *in vivo* studies indicate broad tissue tropism (35). In contrast to a previous study which showed no difference between the permissibility of Calu-3 and Caco-2 cells for SARS-CoV-2 infection (35), the Indian SARS-CoV-2 isolate from our study infected Calu-3 cells better than Caco-2 cells. Interestingly, cell surface expressions of ACE2 on Caco-2 cells was shown to be higher than Calu-3 cells grown on trans-well inserts (36). Therefore, it would be interesting to investigate the difference in ACE2 expression under different growth conditions and passage history of cell lines to correlate with their susceptibility to infection by SARS-CoV-2. Finally, based on previous reports which demonstrate the inhibitory activity of zinc on coronavirus RNA polymerase (28) and the widely accepted beneficial role of zinc supplementation in respiratory infections (37), we show presence of excess zinc was inhibitory to SARS-CoV-2 in Calu-3 cells. As zinc is an acute-phase reactant which undergoes tissue redistribution during infection, our data suggests a beneficial effect of zinc supplementation in COVID-19 infection.

ACKNOWLEDGEMENTS

We thank Amresh Kumar Singh for technical support and all members of CCV lab and bioassay lab for their technical help and critical inputs. We thank all the patients who consented to participate in the study.

AUTHOR CONTRIBUTIONS

AA, SG, SK, JW, NAK, AP, NAK, AK, VA, JSV and RP performed experiments and analyzed the data. AD and AKP coordinated the study at clinical site and contributed reagents. GRM conceived the study, designed the experiments, and analyzed data. AA, SG, SK, JW and GRM wrote the manuscript. All authors have reviewed and approved the final version of the manuscript.

CONFLICT OF INTEREST STATEMENT

The authors declare that they have no conflict of interest to disclose.

FUNDING INFORMATION

This work was supported by funding to GRM by the Biotechnology Industry Research Assistance Council (BIRAC) (BT/NBM0099/02/18). GRM also received funding from the DBT-Wellcome trust India Alliance intermediate fellowship (IA/S/14/1/501291). RP acknowledges funding support from CSIR (MLP-2005), and FondationBotnar (CLP-0031). The funders had no role in study design, data collection and interpretation or the decision to submit the work for publication.

REFERENCES

1. Boni MF, Lemey P, Jiang X, Lam TT, Perry BW, Castoe TA, Rambaut A, Robertson DL. 2020. Evolutionary origins of the SARS-CoV-2 sarbecovirus lineage responsible for the COVID-19 pandemic. Nat Microbiol doi:10.1038/s41564-020-0771-4.

2. Zhou P, Yang XL, Wang XG, Hu B, Zhang L, Zhang W, Si HR, Zhu Y, Li B, Huang CL, Chen HD, Chen J, Luo Y, Guo H, Jiang RD, Liu MQ, Chen Y, Shen XR, Wang X, Zheng XS, Zhao K, Chen QJ, Deng F, Liu LL, Yan B, Zhan FX, Wang YY, Xiao GF, Shi ZL. 2020. A pneumonia outbreak associated with a new coronavirus of probable bat origin. Nature 579:270-273.

3. Hoffmann M, Kleine-Weber H, Schroeder S, Kruger N, Herrler T, Erichsen S, Schiergens TS, Herrler G, Wu NH, Nitsche A, Muller MA, Drosten C, Pohlmann S. 2020. SARS-CoV-2 Cell Entry Depends on ACE2 and TMPRSS2 and Is Blocked by a Clinically Proven Protease Inhibitor. Cell 181:271-280 e8.

4. Wan Y, Shang J, Graham R, Baric RS, Li F. 2020. Receptor Recognition by the Novel Coronavirus from Wuhan: an Analysis Based on Decade-Long Structural Studies of SARS Coronavirus. J Virol 94.

5. Tregoning JS, Brown ES, Cheeseman HM, Flight KE, Higham SL, Lemm NM, Pierce BF, Stirling DC, Wang Z, Pollock KM. 2020. Vaccines for COVID-19. Clin Exp Immunol doi:10.1111/cei.13517.

6. Heimfarth L, Serafini MR, Martins-Filho PR, Quintans JSS, Quintans-Junior LJ. 2020. Drug repurposing and cytokine management in response to COVID-19: A review. Int Immunopharmacol 88:106947.

7. Hadjadj J, Yatim N, Barnabei L, Corneau A, Boussier J, Smith N, Pere H, Charbit B, Bondet V, Chenevier-Gobeaux C, Breillat P, Carlier N, Gauzit R, Morbieu C, Pene F, Marin N, Roche N, Szwebel TA, Merkling SH, Treluyer JM, Veyer D, Mouthon L, Blanc C, Tharaux PL, Rozenberg F, Fischer A, Duffy D, Rieux-Laucat F, Kerneis S, Terrier B.

2020. Impaired type I interferon activity and inflammatory responses in severe COVID-19 patients. Science 369:718-724.

8. Han H, Ma Q, Li C, Liu R, Zhao L, Wang W, Zhang P, Liu X, Gao G, Liu F, Jiang Y, Cheng X, Zhu C, Xia Y. 2020. Profiling serum cytokines in COVID-19 patients reveals IL-6 and IL-10 are disease severity predictors. Emerg Microbes Infect 9:1123-1130.

9. Chen G, Wu D, Guo W, Cao Y, Huang D, Wang H, Wang T, Zhang X, Chen H, Yu H, Zhang X, Zhang M, Wu S, Song J, Chen T, Han M, Li S, Luo X, Zhao J, Ning Q. 2020. Clinical and immunological features of severe and moderate coronavirus disease 2019. J Clin Invest 130:2620-2629.

10. Pujadas E, Chaudhry F, McBride R, Richter F, Zhao S, Wajnberg A, Nadkarni G, Glicksberg BS, Houldsworth J, Cordon-Cardo C. 2020. SARS-CoV-2 viral load predicts COVID-19 mortality. Lancet Respir Med 8:e70.

11. Beigel JH, Tomashek KM, Dodd LE, Mehta AK, Zingman BS, Kalil AC, Hohmann E, Chu HY, Luetkemeyer A, Kline S, Lopez de Castilla D, Finberg RW, Dierberg K, Tapson V, Hsieh L, Patterson TF, Paredes R, Sweeney DA, Short WR, Touloumi G, Lye DC, Ohmagari N, Oh MD, Ruiz-Palacios GM, Benfield T, Fatkenheuer G, Kortepeter MG, Atmar RL, Creech CB, Lundgren J, Babiker AG, Pett S, Neaton JD, Burgess TH, Bonnett T, Green M, Makowski M, Osinusi A, Nayak S, Lane HC, Members A-SG. 2020. Remdesivir for the Treatment of Covid-19 - Final Report. N Engl J Med doi:10.1056/NEJMoa2007764.

12. Zhao Z, Li H, Wu X, Zhong Y, Zhang K, Zhang YP, Boerwinkle E, Fu YX. 2004. Moderate mutation rate in the SARS coronavirus genome and its implications. BMC Evol Biol 4:21.

562 13. Forni D, Cagliani R, Clerici M, Sironi M. 2017. Molecular Evolution of Human
563 Coronavirus Genomes. Trends Microbiol 25:35-48.
564 14. Koyama T, Platt D, Parida L. 2020. Variant analysis of SARS-CoV-2 genomes. Bull World
565 Health Organ 98:495-504.
566 15. Zhang X, Tan Y, Ling Y, Lu G, Liu F, Yi Z, Jia X, Wu M, Shi B, Xu S, Chen J, Wang W,
567 Chen B, Jiang L, Yu S, Lu J, Wang J, Xu M, Yuan Z, Zhang Q, Zhang X, Zhao G, Wang
568 S, Chen S, Lu H. 2020. Viral and host factors related to the clinical outcome of COVID-
569 19. Nature 583:437-440.
570 16. Agrawal T, Schu P, Medigeshi GR. 2013. Adaptor protein complexes-1 and 3 are involved
571 at distinct stages of flavivirus life-cycle. Sci Rep 3:1813.
572 17. Kar M, Khan NA, Panwar A, Bais SS, Basak S, Goel R, Sopory S, Medigeshi GR. 2019.
573 Zinc Chelation Specifically Inhibits Early Stages of Dengue Virus Replication by
574 Activation of NF-kappaB and Induction of Antiviral Response in Epithelial Cells. Front
575 Immunol 10:2347.
576 18. Kumar P, Pandey R, Sharma P, Dhar M, A. V, Uppili B, Vashisht H, Wadhwa S, Tyagi N,
577 Fatihi S, Sharma U, Singh P, Lall H, Datta M, Gupta P, Saini N, Tewari A, Nandi B, Kumar
578 D, Bag S, Gahlot D, Rathore S, Jatana N, Jaiswal V, Gogia H, Madan P, Singh S, Singh P,
579 Dash D, Bala M, Kabra S, Singh S, Mukerji M, Thukral L, Faruq M, Agrawal A, Rakshit
580 P. 2020. Integrated genomic view of SARS-CoV-2 in India [version 1; peer review: 2
581 approved]. Wellcome Open Research 5.
582 19. Quick J, Grubaugh ND, Pullan ST, Claro IM, Smith AD, Gangavarapu K, Oliveira G,
583 Robles-Sikisaka R, Rogers TF, Beutler NA, Burton DR, Lewis-Ximenez LL, de Jesus JG,
584 Giovanetti M, Hill SC, Black A, Bedford T, Carroll MW, Nunes M, Alcantara LC, Jr.,

585 Sabino EC, Baylis SA, Faria NR, Loose M, Simpson JT, Pybus OG, Andersen KG, Loman
586 NJ. 2017. Multiplex PCR method for MinION and Illumina sequencing of Zika and other
587 virus genomes directly from clinical samples. Nat Protoc 12:1261-1276.
588 20. Li H. 2018. Minimap2: pairwise alignment for nucleotide sequences. Bioinformatics
589 34:3094-3100.
590 21. Loman NJ, Quick J, Simpson JT. 2015. A complete bacterial genome assembled de novo
591 using only nanopore sequencing data. Nat Methods 12:733-5.
592 22. Edgar RC. 2004. MUSCLE: multiple sequence alignment with high accuracy and high
593 throughput. Nucleic Acids Res 32:1792-7.
594 23. Price MN, Dehal PS, Arkin AP. 2010. FastTree 2--approximately maximum-likelihood
595 trees for large alignments. PLoS One 5:e9490.
596 24. Letunic I, Bork P. 2019. Interactive Tree Of Life (iTOL) v4: recent updates and new
597 developments. Nucleic Acids Res 47:W256-W259.
598 25. Braakhuis HM, He R, Vandebriel RJ, Gremmer ER, Zwart E, Vermeulen JP, Fokkens P,
599 Boere J, Gosens I, Cassee FR. 2020. An Air-liquid Interface Bronchial Epithelial Model
600 for Realistic, Repeated Inhalation Exposure to Airborne Particles for Toxicity Testing. J
601 Vis Exp doi:10.3791/61210.
602 26. Matsuyama S, Nao N, Shirato K, Kawase M, Saito S, Takayama I, Nagata N, Sekizuka T,
603 Katoh H, Kato F, Sakata M, Tahara M, Kutsuna S, Ohmagari N, Kuroda M, Suzuki T,
604 Kageyama T, Takeda M. 2020. Enhanced isolation of SARS-CoV-2 by TMPRSS2-
605 expressing cells. Proc Natl Acad Sci U S A 117:7001-7003.
606 27. Korber B, Fischer WM, Gnanakaran S, Yoon H, Theiler J, Abfalterer W, Hengartner N,
607 Giorgi EE, Bhattacharya T, Foley B, Hastie KM, Parker MD, Partridge DG, Evans CM,

608 Freeman TM, de Silva TI, Sheffield C-GG, McDanal C, Perez LG, Tang H, Moon-Walker
609 A, Whelan SP, LaBranche CC, Saphire EO, Montefiori DC. 2020. Tracking Changes in
610 SARS-CoV-2 Spike: Evidence that D614G Increases Infectivity of the COVID-19 Virus.
611 Cell 182:812-827 e19.
612 28. te Velthuis AJ, van den Worm SH, Sims AC, Baric RS, Snijder EJ, van Hemert MJ. 2010.
613 Zn(2+) inhibits coronavirus and arterivirus RNA polymerase activity in vitro and zinc
614 ionophores block the replication of these viruses in cell culture. PLoS Pathog 6:e1001176.
615 29. Chu H, Chan JF, Wang Y, Yuen TT, Chai Y, Hou Y, Shuai H, Yang D, Hu B, Huang X,
616 Zhang X, Cai JP, Zhou J, Yuan S, Kok KH, To KK, Chan IH, Zhang AJ, Sit KY, Au WK,
617 Yuen KY. 2020. Comparative Replication and Immune Activation Profiles of SARS-CoV-
618 2 and SARS-CoV in Human Lungs: An Ex Vivo Study With Implications for the
619 Pathogenesis of COVID-19. Clin Infect Dis 71:1400-1409.
620 30. Blanco-Melo D, Nilsson-Payant BE, Liu WC, Uhl S, Hoagland D, Moller R, Jordan TX,
621 Oishi K, Panis M, Sachs D, Wang TT, Schwartz RE, Lim JK, Albrecht RA, tenOever BR.
622 2020. Imbalanced Host Response to SARS-CoV-2 Drives Development of COVID-19.
623 Cell 181:1036-1045 e9.
624 31. Felgenhauer U, Schoen A, Gad HH, Hartmann R, Schaubmar AR, Failing K, Drosten C,
625 Weber F. 2020. Inhibition of SARS-CoV-2 by type I and type III interferons. J Biol Chem
626 295:13958-13964.
627 32. Groeneveld ABJ. A Central Role of Interleukin-8 in the Pathogenesis of ARDS, p 65-74.
628 *In* (ed), Springer Berlin Heidelberg,
629 33. Galani IE, Andreakos E. 2015. Neutrophils in viral infections: Current concepts and
630 caveats. J Leukoc Biol 98:557-64.

34. Sarkale P, Patil S, Yadav PD, Nyayanit DA, Sapkal G, Baradkar S, Lakra R, Shete-Aich A, Prasad S, Basu A, Dar L, Vipat V, Giri S, Potdar V, Choudhary ML, Praharaj I, Jain A, Malhotra B, Gawande P, Kalele K, Gupta N, Cherian SS, Abraham P. 2020. First isolation of SARS-CoV-2 from clinical samples in India. Indian J Med Res 151:244-250.

35. Chu H, Chan JF, Yuen TT, Shuai H, Yuan S, Wang Y, Hu B, Yip CC, Tsang JO, Huang X, Chai Y, Yang D, Hou Y, Chik KK, Zhang X, Fung AY, Tsoi HW, Cai JP, Chan WM, Ip JD, Chu AW, Zhou J, Lung DC, Kok KH, To KK, Tsang OT, Chan KH, Yuen KY. 2020. Comparative tropism, replication kinetics, and cell damage profiling of SARS-CoV-2 and SARS-CoV with implications for clinical manifestations, transmissibility, and laboratory studies of COVID-19: an observational study. Lancet Microbe 1:e14-e23.

36. Ren X, Glende J, Al-Falah M, de Vries V, Schwegmann-Wessels C, Qu X, Tan L, Tschernig T, Deng H, Naim HY, Herrler G. 2006. Analysis of ACE2 in polarized epithelial cells: surface expression and function as receptor for severe acute respiratory syndrome-associated coronavirus. J Gen Virol 87:1691-5.

37. Lassi ZS, Moin A, Bhutta ZA. 2016. Zinc supplementation for the prevention of pneumonia in children aged 2 months to 59 months. Cochrane Database Syst Rev 12:CD005978.

SUPPLEMENTARY INFORMATION

This article has supplementary information.

652 **TABLE**

653 **Table – 1 List of mutations in plaque-purified isolates compared to the reference Wuhan**

654 **strain (MN908947.3).**

Virus	Nucleotide position	Base change	Open reading frame	Amino acid substitution
THSTI-2010-(A, B, C, D)	1227	T→C	ORF1a	M321T
	1281	C→T	ORF1a	A339V
	1758	C→T	ORF1a	A498V
	4885	T→C	ORF1a	Synonymous
	6312	C→A	ORF1a	T2016K
	11083	G→T	ORF1a	L3606F
	13730	C→T	ORF1b	A88V
	23929	C→T	Surface glycoprotein (S; Spike)	Synonymous
	28311	C→T	Nucleocapsid phosphoprotein (N)	P13L
THSTI-2010-C	27806	G→T	ORF7b	Synonymous

655

656 **FIGURE LEGENDS**

657 **Figure 1: Kinetics of viral load in VTM and saliva samples of COVID-19 patients.** A-F)

658 SARS-CoV-2 RNA levels were measured by RT-PCR using total RNA isolated from VTM

samples every day after enrolment. G-K) SARS-CoV-2 RNA levels were measured by RT-PCR using total RNA isolated from saliva and VTM samples every day after enrolment. Data points indicate geometric mean normalized to RNASe P levels which was used as endogenous controls for extraction efficiency.

Figure 2: Kinetics of secreted inflammatory mediators in COVID-19 patients. A) Daily IFN-α, IFN-γ levels (on the left y-axis) were estimated from serum samples of COVID-19 patients using luminex assays and copy numbers of viral genome equivalents (on the right-y axis) was estimated from RNA isolated from VTM samples every day. B) The levels of indicated cytokines influencing T-cell functions were estimated from serum samples collected daily from COVID-19 patients. C) The levels of indicated chemokines suggestive of inflammation were estimated from serum samples collected daily from COVID-19 patients. D) The levels of indicated cytokines which are key determinants of inflammatory response were estimated from serum samples collected daily from COVID-19 patients. Columns indicate the median value with 95% CI.

Figure 3: THSTI-BL-2010 plaque-purified isolates. A) Single plaque morphology of THSTI-BL-2010 at 72 h pi. Virus from four single plaques were propagated on VeroE6 monolayer separately. Cytopathic effect was evident at 72 h post-infection for all the four isolates. Images were captured at 20X magnification. B) VeroE6 cells were used for performing plaque assays with either the reference SARS-CoV-2 strain or THSTI-BL-2010D.Cells were fixed at 60 h pi and stained with crystal violet.

Figure 4: Infection of human cell lines. A) Vero E6, Calu-3 and Caco-2 cells were either mock-infected or infected with THSTI-2010-D at indicated MOI for 24 h. Cells were fixed in and stained with anti-spike protein antibody and probed with secondary antibody conjugated with Alexa Fluor 488. Images were captured using Olympus DP80 microscope. Scale bar is 100 µm. B) Growth curve of SARS-CoV-2 Wuhan and THSTI-BL2010D strain were compared on Vero E6 cells. Vero E6 cells were infected at 0.1 MOI either with Wuhan strain or THSTI BL2010D. Viral titers were measured at 24 h, 48 h and 72 h in culture supernatants (n=3).

Figure 5. Maximum likelihood phylogeny for SARS CoV2 sequences (n=100). Indian isolates reported here falls under 19A clade. The sequence of plaque purified isolates are highlighted with symbol 'star'. The GISAID clades are indicated as mentioned in the inset. The scale bar indicates the branch lengths measured in number of nucleotide substitution rate per site.

Figure 6: SARS-CoV-2 infection disrupts epithelial barrier integrity. A) Calu-3 cells grown on transwells at air-liquid interface as described in methods section. Polarized Calu-3 cells were infected with SARS-CoV-2 THSTI-BL-2010D at 0.3 MOI. TEER was measured at 24 h pi. TEER values were represented as ohm/cm^2. B) Viral titres were determined at 24 h pi and represented as pfu/ml. C) Cells were fixed and stained with ZO-1 and Claudin-3 antibodies against cellular junctions and spike antibody against viral protein. Nuclei were stained with DAPI. Images were captured at 100X. Representative images of mock and SARS-CoV-2 infected cells are displayed. Scale bar is 10 µm. D) Calu-3 cells were treated with indicated concentrations of $ZnSO_4$ for 24 h and cell viability was measured using CellTiter-Glo® Assay kit. E) Calu-3 cells were infected with SARS-CoV-2-THSTI-BL-2010D at 0.3 MOI. After viral

adsorption, cells were treated with 25 and 50 μM of $ZnSO_4$ or as mock treated control. Viral titres were determined as represented as pfu/ml. (n=3). Error bars represent mean ± SD. *p < 0.05, **p < 0.01.

SUPPLEMENTARY FIGURE LEGENDS

Figure S1: SARS-CoV-2 Indian isolates. Vero E6 cells were infected with nasopharyngeal swab samples for 1 h and cultured in growth medium thereafter. CPE was evident at 48 h post-infection. Images were captured using Nikon Eclipse Ti-S microscope at 20X magnification.

Figure S2: Zinc uptake in Calu-3 cells. Calu-3 cells after incubation with indicated concentrations of zinc sulfate for 4 h and labile zinc levels were measured by staining with ZinPyr-1 and flow cytometry. The relative change in the mean fluorescence intensities of ZP-1 is shown in the graph. Error bars represent Mean with SD.

Figure 1

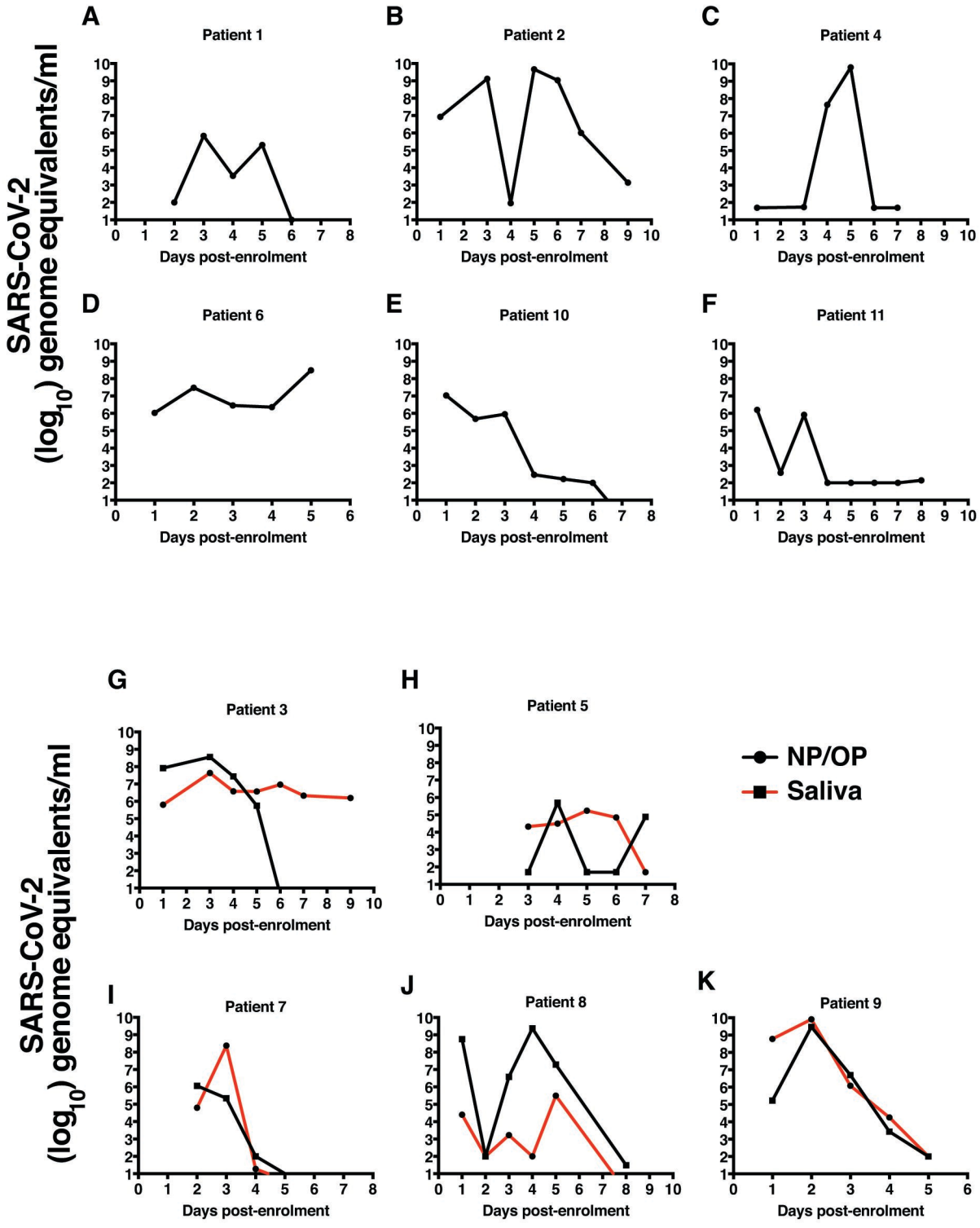
A
Patient 1
B
Patient 2
C
Patient 4
D
Patient 6
E
Patient 10
F
Patient 11
G
Patient 3
H
Patient 5
I
Patient 7
J
Patient 8
K
Patient 9
SARS-CoV-2 (log10) genome equivalents/ml
Days post-enrolment
NP/OP
Saliva

Figure 2

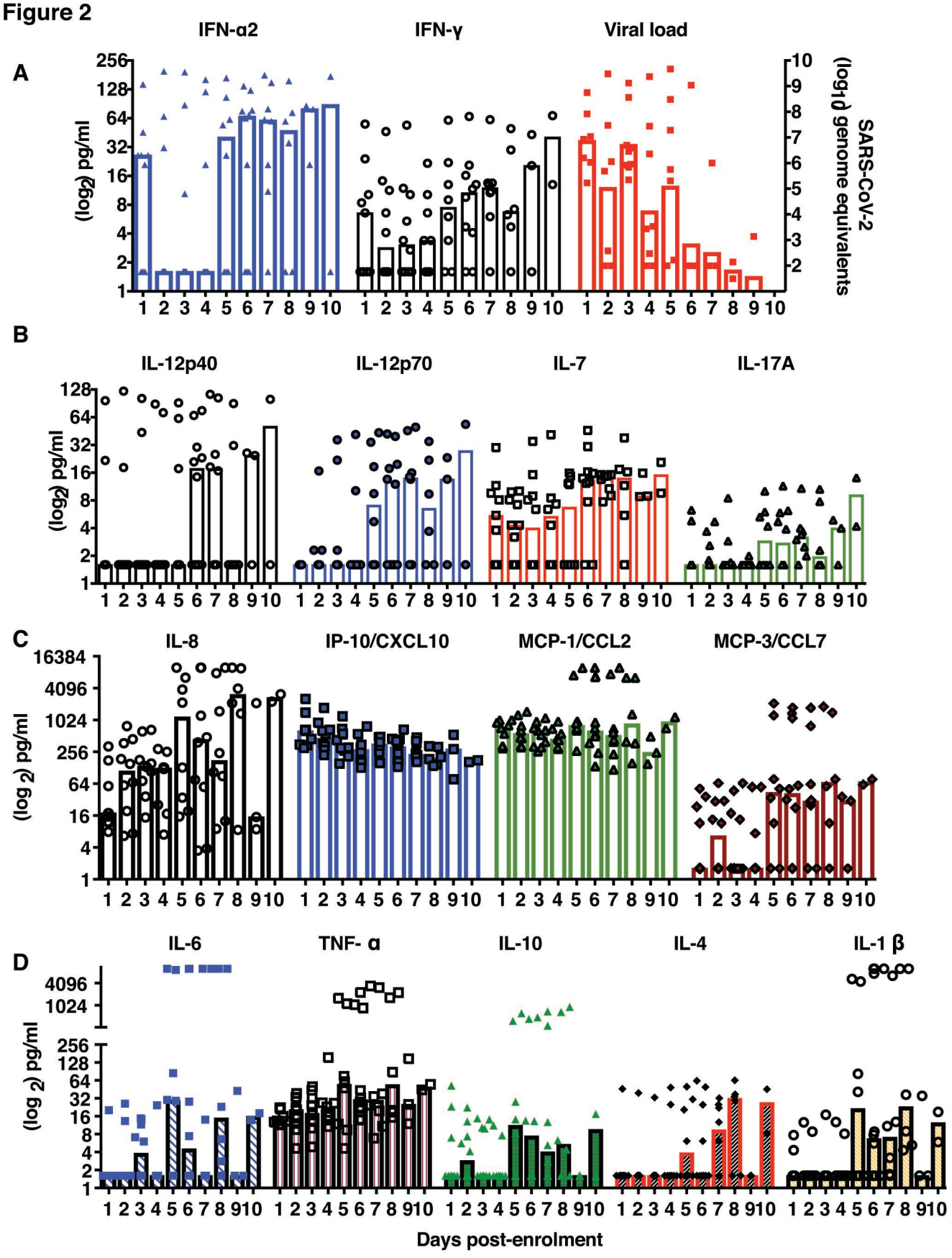
A
IFN-α2
IFN-γ
Viral load
(log2) pg/ml
(log10) genome equivalents SARS-CoV-2
B
IL-12p40
IL-12p70
IL-7
IL-17A
(log2) pg/ml
C
IL-8
IP-10/CXCL10
MCP-1/CCL2
MCP-3/CCL7
(log 2) pg/ml
D
IL-6
TNF- α
IL-10
IL-4
IL-1 β
(log 2) pg/ml
Days post-enrolment

Figure 3

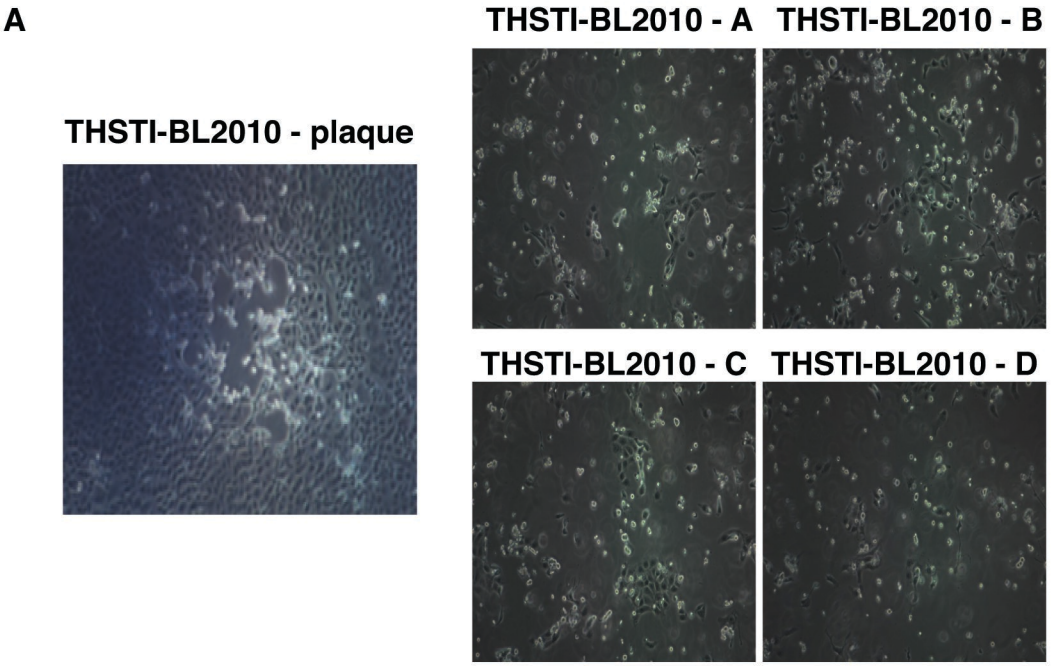
A
THSTI-BL2010 - plaque
THSTI-BL2010 - A
THSTI-BL2010 - B
THSTI-BL2010 - C
THSTI-BL2010 - D

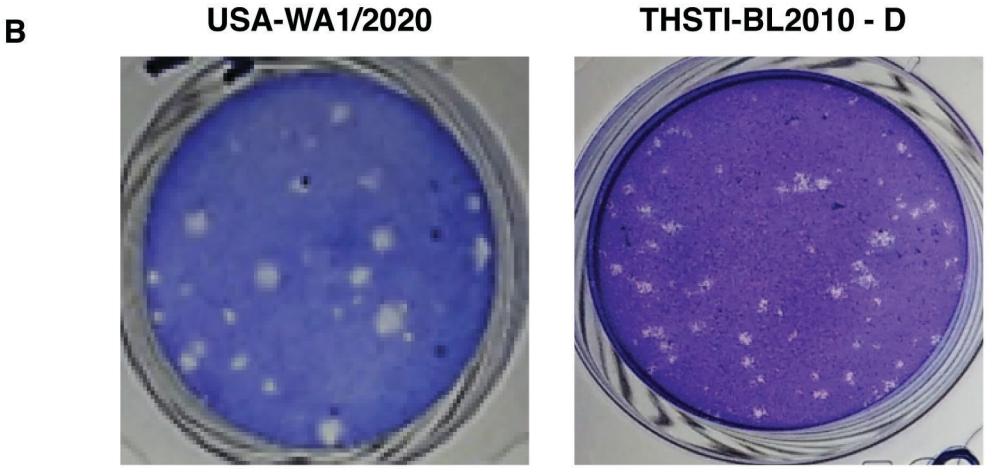
B
USA-WA1/2020
THSTI-BL2010 - D

Figure 4

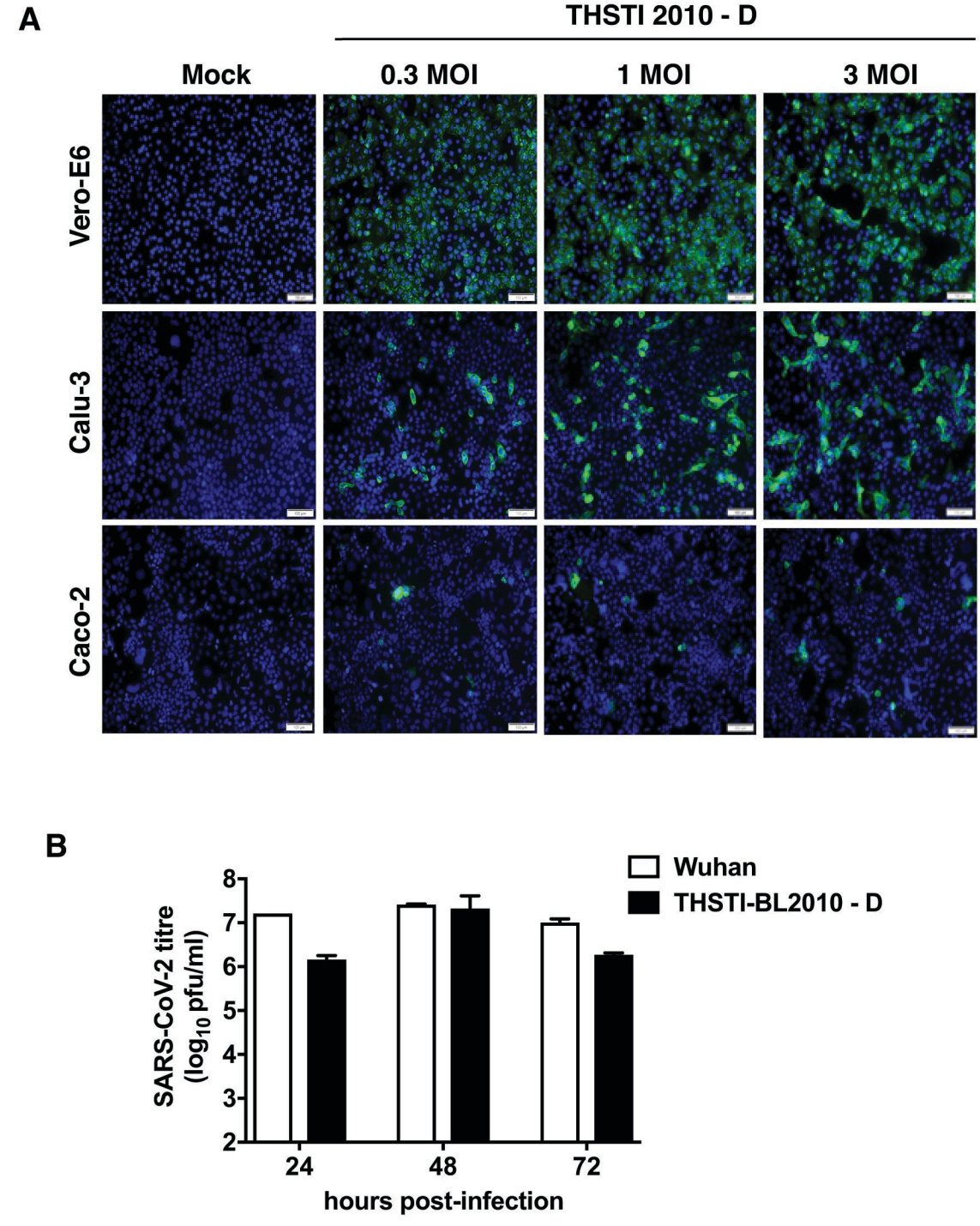
A
THSTI 2010 - D
Mock
0.3 MOI
1 MOI
3 MOI
Vero-E6
Calu-3
Caco-2
B
Wuhan
THSTI-BL2010 - D
SARS-CoV-2 titre
(log10 pfu/ml)
8
7
6
5
4
3
2
24
48
72
hours post-infection

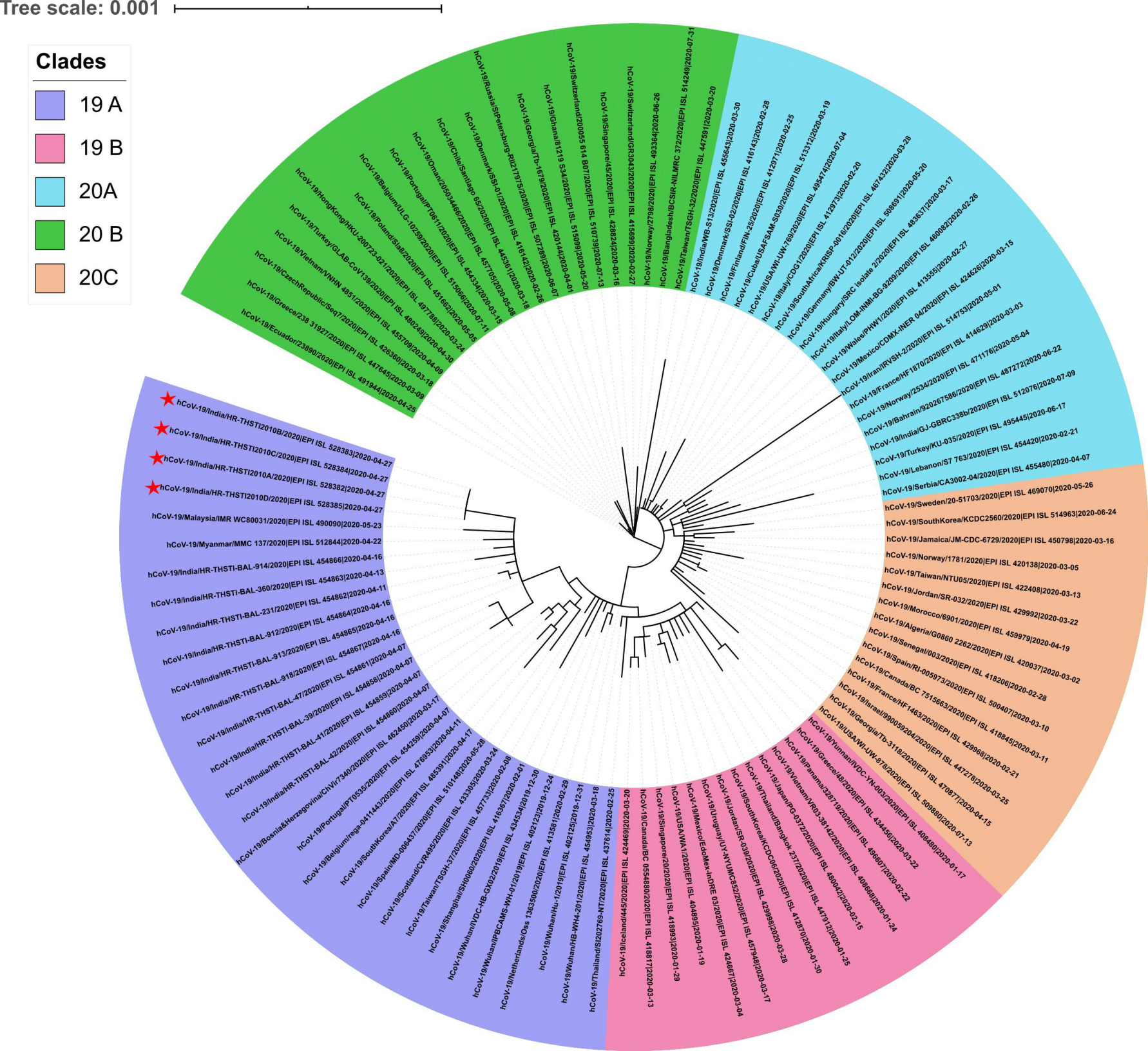
Tree scale: 0.001
Clades
19 A
19 B
20A
20 B
20C
hCoV-19/India/HR-THSTI2010B/2020|EPI ISL 528383|2020-04-27
hCoV-19/India/HR-THSTI2010C/2020|EPI ISL 528384|2020-04-27
hCoV-19/India/HR-THSTI2010A/2020|EPI ISL 528382|2020-04-27
hCoV-19/India/HR-THSTI2010D/2020|EPI ISL 528385|2020-04-27
hCoV-19/Malaysia/IMR WC80031/2020|EPI ISL 490090|2020-05-23
hCoV-19/Myanmar/MMC 137/2020|EPI ISL 512844|2020-04-22
hCoV-19/India/HR-THSTI-BAL-914/2020|EPI ISL 454866|2020-04-16
hCoV-19/India/HR-THSTI-BAL-360/2020|EPI ISL 454863|2020-04-13
hCoV-19/India/HR-THSTI-BAL-231/2020|EPI ISL 454862|2020-04-11
hCoV-19/India/HR-THSTI-BAL-912/2020|EPI ISL 454864|2020-04-16
hCoV-19/India/HR-THSTI-BAL-913/2020|EPI ISL 454865|2020-04-16
hCoV-19/India/HR-THSTI-BAL-918/2020|EPI ISL 454867|2020-04-16
hCoV-19/India/HR-THSTI-BAL-47/2020|EPI ISL 454861|2020-04-07
hCoV-19/India/HR-THSTI-BAL-39/2020|EPI ISL 454858|2020-04-07
hCoV-19/India/HR-THSTI-BAL-41/2020|EPI ISL 454859|2020-04-07
hCoV-19/India/HR-THSTI-BAL-42/2020|EPI ISL 454860|2020-04-07
hCoV-19/Bosnia&Herzegovina/ChVir7340/2020|EPI ISL 462450|2020-03-17
hCoV-19/Portugal/PT0535/2020|EPI ISL 454259|2020-04-07
hCoV-19/Belgium/rega-0411443/2020|EPI ISL 476953|2020-04-17
hCoV-19/SouthKorea/A17/2020|EPI ISL 485391|2020-04-17
hCoV-19/Spain/IMD-0064337/2020|EPI ISL 510148|2020-05-28
hCoV-19/Scotland/CVR495/2020|EPI ISL 433305|2020-03-24
hCoV-19/Taiwan/TSGH-37/2020|EPI ISL 457733|2020-02-08
hCoV-19/Shanghai/SH0060/2020|EPI ISL 416367|2020-02-01
hCoV-19/Wuhan/IVDC-HB-GX02/2019|EPI ISL 434534|2019-12-30
hCoV-19/Wuhan/IPBCAMS-WH-01/2019|EPI ISL 402123|2019-12-24
hCoV-19/Netherlands/Oss 1363500/2020|EPI ISL 413681|2020-02-29
hCoV-19/Wuhan/Hu-1/2019|EPI ISL 402125|2019-12-31
hCoV-19/Wuhan/HB-WH4-201/2020|EPI ISL 454953|2020-03-18
hCoV-19/Thailand/SI202769-NT/2020|EPI ISL 437614|2020-02-25
hCoV-19/Iceland/445/2020|EPI ISL 424469|2020-03-20
hCoV-19/Canada/BC 0554880/2020|EPI ISL 418817|2020-03-13
hCoV-19/Singapore/20/2020|EPI ISL 418993|2020-01-29
hCoV-19/USA/WA1/2020|EPI ISL 404895|2020-01-19
hCoV-19/Mexico/EdoMex-InDRE 03/2020|EPI ISL 424667|2020-03-04
hCoV-19/Uruguay/UY-NYUMC852/2020|EPI ISL 457948|2020-03-17
hCoV-19/Jordan/SR-039/2020|EPI ISL 429999|2020-03-28
hCoV-19/SouthKorea/KCDC09/2020|EPI ISL 412870|2020-01-30
hCoV-19/Thailand/BangkoK 237/2020|EPI ISL 448042|2020-02-15
hCoV-19/Japan/PG-0372/2020|EPI ISL 448791|2020-01-25
hCoV-19/VietnamVR03-38142/2020|EPI ISL 408668|2020-01-24
hCoV-19/Panama/328719/2020|EPI ISL 496607|2020-02-22
hCoV-19/Greece/48/2020|EPI ISL 434456|2020-03-22
hCoV-19/Yunnan/IVDC-YN-003/2020|EPI ISL 408480|2020-01-17
hCoV-19/USA/WI-UW-978/2020|EPI ISL 509980|2020-07-13
hCoV-19/Georgia/Tb-3118/2020|EPI ISL 470877|2020-04-15
hCoV-19/Israel/9900592O4/2020|EPI ISL 447278|2020-03-25
hCoV-19/France/HF1463/2020|EPI ISL 429968|2020-02-21
hCoV-19/Canada/BC 7515663/2020|EPI ISL 418845|2020-03-11
hCoV-19/Canada/RI-005973/2020|EPI ISL 500407|2020-03-10
hCoV-19/Spain/2020|EPI ISL 418206|2020-02-28
hCoV-19/Senegal/003/2020|EPI ISL 420037|2020-03-02
hCoV-19/Algeria/G0860 2262/2020|EPI ISL 459979|2020-04-19
hCoV-19/Morocco/6901/2020|EPI ISL 429992|2020-03-22
hCoV-19/Jordan/SR-032/2020|EPI ISL 422408|2020-03-13
hCoV-19/Taiwan/NTU05/2020|EPI ISL 422408|2020-03-13
hCoV-19/Norway/1781/2020|EPI ISL 420138|2020-03-05
hCoV-19/Jamaica/JM-CDC-6729/2020|EPI ISL 450798|2020-03-16
hCoV-19/SouthKorea/KCDC2560/2020|EPI ISL 514963|2020-06-24
hCoV-19/Sweden/20-51703/2020|EPI ISL 469070|2020-05-26
hCoV-19/Serbia/CA3002-04/2020|EPI ISL 455480|2020-04-07
hCoV-19/Lebanon/S7 763/2020|EPI ISL 454420|2020-02-21
hCoV-19/Turkey/KU-035/2020|EPI ISL 495445|2020-06-17
hCoV-19/India/GJ-GBRC338b/2020|EPI ISL 512076|2020-07-09
hCoV-19/Bahrain/920267586/2020|EPI ISL 487272|2020-06-22
hCoV-19/Norway/2534/2020|EPI ISL 471176|2020-05-04
hCoV-19/France/HF1870/2020|EPI ISL 414629|2020-03-03
hCoV-19/Iran/IRVSH-2/2020|EPI ISL 514753|2020-05-01
hCoV-19/Mexico/CDMX-INER 04/2020|EPI ISL 424626|2020-03-15
hCoV-19/Wales/PHW1/2020|EPI ISL 413555|2020-02-27
hCoV-19/Italy/LOM-INMI-BG-9209/2020|EPI ISL 460082|2020-02-26
hCoV-19/Hungary/SRC isolate 2/2020|EPI ISL 483637|2020-03-17
hCoV-19/Germany/BW-UT-012/2020|EPI ISL 508691|2020-05-20
hCoV-19/SouthAfrica/KRISP-0016/2020|EPI ISL 467432|2020-03-28
hCoV-19/Italy/CDG1/2020|EPI ISL 412973|2020-02-20
hCoV-19/USA/WI-UW-769/2020|EPI ISL 495474|2020-07-04
hCoV-19/Cuba/USAFSAM-S030/2020|EPI ISL 513312|2020-03-19
hCoV-19/Finland/FIN-23/2020|EPI ISL 412971|2020-02-25
hCoV-19/Denmark/SSI-02/2020|EPI ISL 416143|2020-02-28
hCoV-19/India/WB-S13/2020|EPI ISL 455643|2020-03-30
hCoV-19/Taiwan/TSGH-32/2020|EPI ISL 447591|2020-03-20
hCoV-19/Bangladesh/BCSIR-NIILMRC 372/2020|EPI ISL 514249|2020-07-31
hCoV-19/Norway/27986/2020|EPI ISL 493964|2020-06-26
hCoV-19/Switzerland/GR30432/2020|EPI ISL 415699|2020-02-27
hCoV-19/Singapore/45/2020|EPI ISL 428824|2020-03-16
hCoV-19/Switzerland/200055 614 B07/2020|EPI ISL 510739|2020-07-13
hCoV-19/Ghana/81219 S34/2020|EPI ISL 420144|2020-04-01
hCoV-19/Georgia/Tb-1679/2020|EPI ISL 507289|2020-06-07
hCoV-19/Russia/StPetersburg-RII21791S/2020|EPI ISL 416142|2020-02-26
hCoV-19/Denmark/SSI-01/2020|EPI ISL 445361|2020-03-18
hCoV-19/Chile/Santiago 65/2020|EPI ISL 457705|2020-05-08
hCoV-19/Oman/20S03466/2020|EPI ISL 454334|2020-03-15
hCoV-19/Portugal/PT0611/2020|EPI ISL 451662|2020-05-05
hCoV-19/Belgium/ULG-10259/2020|EPI ISL 515068|2020-07-11
hCoV-19/Poland/Sia8/2020|EPI ISL 497788|2020-03-24
hCoV-19/HongKong/HKU-200723-021/2020|EPI ISL 480249|2020-04-30
hCoV-19/Turkey/GLAB-CoV139/2020|EPI ISL 455709|2020-04-09
hCoV-19/Vietnam/VNHN 4851/2020|EPI ISL 426360|2020-03-18
hCoV-19/CzechRepublic/Seq7/2020|EPI ISL 447645|2020-03-09
hCoV-19/Greece/238 31927/2020|EPI ISL 491944|2020-04-25
hCoV-19/Ecuador/23890/2020|EPI ISL 491944|2020-04-25

Figure 6

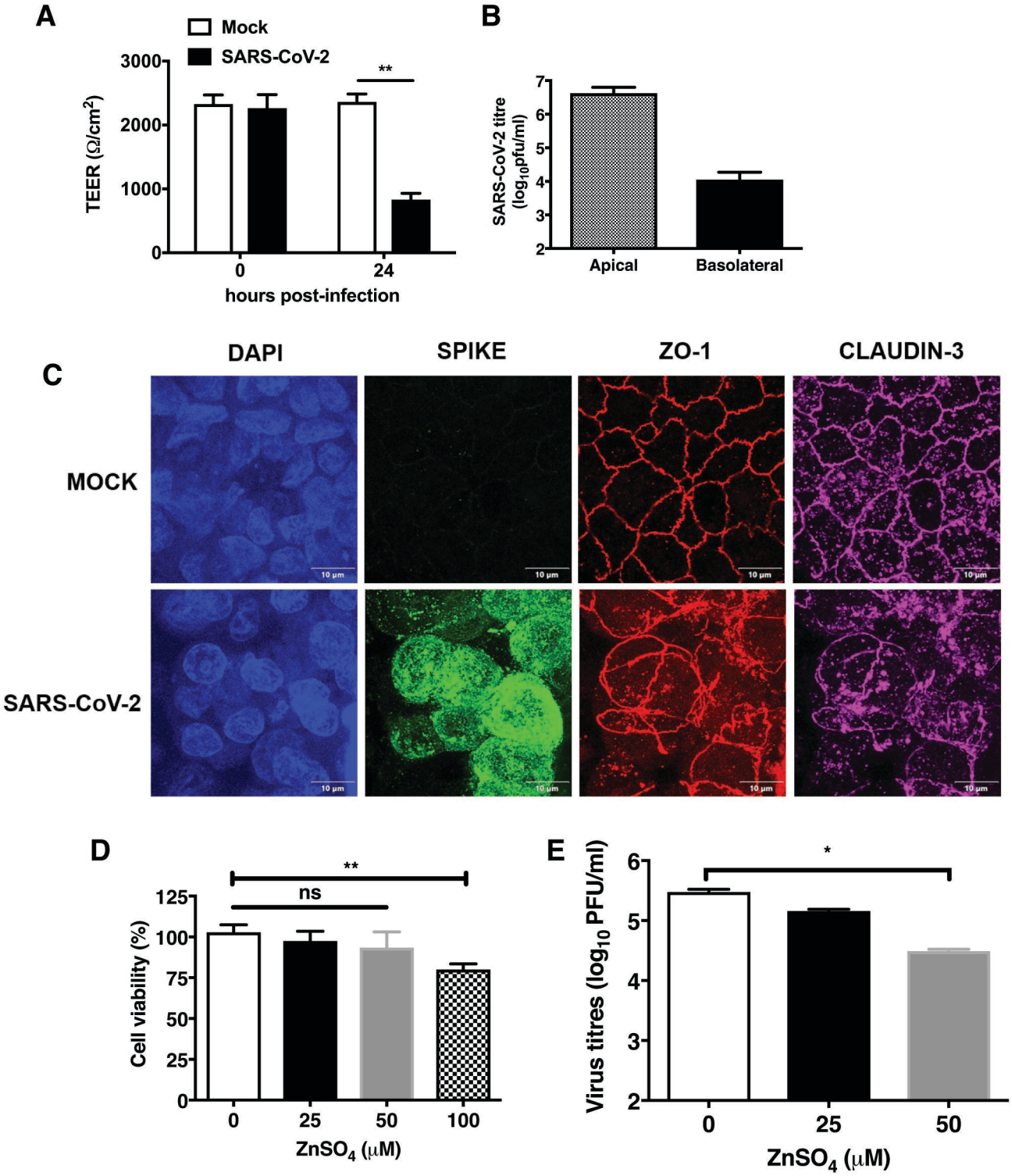
A
Mock
SARS-CoV-2
**
TEER (Ω/cm²)
3000
2000
1000
0
0
24
hours post-infection
B
SARS-CoV-2 titre (log10pfu/ml)
7
6
5
4
3
2
Apical
Basolateral
C
DAPI
SPIKE
ZO-1
CLAUDIN-3
MOCK
SARS-CoV-2
10 µm
D
**
ns
Cell viability (%)
125
100
75
50
25
0
0
25
50
100
ZnSO4 (µM)
E
*
Virus titres (log10 PFU/ml)
6
5
4
3
2
0
25
50
ZnSO4 (µM)